ACS Macro Letters

Letter

pubs.acs.org/macroletters

Signatures of Multiphase Formation in the Active Layer of Organic Solar Cells from Resonant Soft X-ray Scattering

Changhe Guo,[†] Derek R. Kozub,[†] Sameer Vajjala Kesava,[†] Cheng Wang,[‡] Alexander Hexemer,[‡] and Enrique D. Gomez*[,†,§]

[†]Department of Chemical Engineering, The Pennsylvania State University, University Park, Pennsylvania 16802, United States

[‡]Advanced Light Source, Lawrence Berkeley National Laboratory, Berkeley, California 94720, United States

[§]Materials Research Institute, The Pennsylvania State University, University Park, Pennsylvania 16802, United States

Supporting Information

ABSTRACT: Resonant soft X-ray scattering (RSOXS) is a complementary tool to existing reciprocal space methods, such as grazing-incidence small-angle X-ray scattering, for studying order formation in polymer thin films. In particular, RSOXS can exploit differences in absorption between multiple phases by tuning the X-ray energy to one or more resonance peaks of organic materials containing carbon, oxygen, nitrogen, or other atoms. Here, we have examined the structural evolution in poly(3-hexylthiophene-2,5-diyl)/[6,6]-phenyl-C_{61}-butyric acid methyl ester mixtures by tuning X-rays to resonant absorption energies of carbon and oxygen. Our studies reveal that the energy dependence of RSOXS profiles marks the formation of multiple phases in the active layer of organic solar cells, which is consistent with elemental maps obtained through energy-filtered transmission electron microscopy.

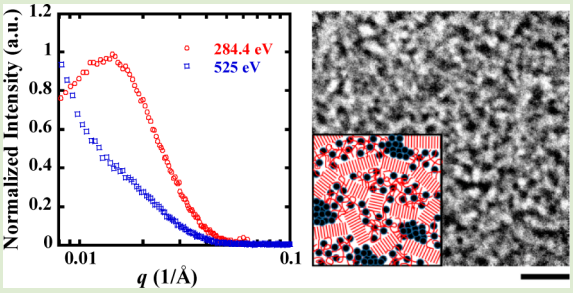

Solution-processed organic photovoltaics (OPVs) have the potential to produce large-scale, low-cost, and renewable power in the form of flexible thin films.[1] Currently, OPV devices with the highest performance are based on the bulk heterojunction architecture,[2] where spontaneous phase separation of electron donor and acceptor materials forms the morphology necessary for high-performance organic solar cells.[3] Many reports have explored control of the nanostructure through a variety of processing approaches, including varying the blend ratio,[4] choice of solvent,[5] thermal and solvent annealing,[6] and the inclusion of additives.[7] Nevertheless, our ability to correlate these factors with OPV performance is limited due to the lack of techniques for building a detailed analysis of the morphology.

Many recent efforts have focused on the characterization of phase separation in the active layer of organic solar cells.[3c,8] In the most studied devices comprised of poly(3-hexylthiophene-2,5-diyl) (P3HT) and [6,6]-phenyl-C_{61}-butyric acid methyl ester (PCBM), structure formation has been studied via scanning probe microscopy (SPM),[9] transmission electron microscopy (TEM),[8f,9b,10] and scattering techniques.[8a,11] However, mass contrast is weak in TEM images, and SPM techniques like atomic force microscopy require surface contrast to provide topographic images yielding limited information. We have previously utilized energy-filtered transmission electron microscopy (EFTEM) and grazing-incidence small-angle X-ray scattering (GISAXS) to examine the morphological evolution in P3HT/PCBM mixtures.[8e] EFTEM couples spectroscopy and microscopy to significantly improve the contrast and map the local elemental composition by imaging with inelastically scattered electrons. GISAXS can quantitatively characterize the structure in thin films of organic semiconductor mixtures. The chemical sensitivity of GISAXS is limited, however, which limits the application of this technique for blends with little mass contrast or in complicated multiphase systems.

In this Letter, we demonstrate that resonant soft X-ray scattering (RSOXS) is an important complementary tool to existing reciprocal space methods for characterizing the morphology in organic thin films. The use of RSOXS for block copolymers and polymer/polymer mixtures has shown greatly enhanced scattering intensity over conventional hard X-ray scattering.[12] Utilizing X-ray energies that match the core electron transitions of the constituent atoms in organic materials enables RSOXS to provide elemental selectivity and chemical sensitivity to exploit differences in absorption between multiple phases. Here, we report the application of RSOXS coupled with EFTEM to characterize the phase separation in P3HT/PCBM mixtures, which are commonly utilized as the active layer of organic solar cells, by tuning the X-ray energy to the absorption edges of carbon and oxygen. We demonstrate the ability of RSOXS to characterize multiphase formation in organic semiconductor mixtures, which is beyond the

Received: October 18, 2012
Accepted: January 29, 2013
Published: February 14, 2013

capabilities of GISAXS, using P3HT/PCBM films as a model system.

In the soft X-ray spectrum (200−2000 eV) where absorption is significant for organic materials, the amplitude of the scattered field from each phase scales strongly with its complex refractive index $n(\lambda)$, which is composed of a dispersive component $\delta(\lambda)$ and an absorptive component $\beta(\lambda)$.[13] The scattering contrast arises from the difference in $n(\lambda)$, or $\delta(\lambda)$ and $\beta(\lambda)$, between different phases as described in eq 1[12b]

$$I \propto \frac{\Delta n \Delta n^*}{\lambda^4} = \frac{(\Delta\beta)^2 + (\Delta\delta)^2}{\lambda^4} \quad (1)$$

where Δn is the difference in $n(\lambda)$ between two phases and Δn^* is the complex conjugate of Δn. Because the energies of the core levels (1s) of carbon, nitrogen, and oxygen are located in the soft X-ray range, energy resolutions near 0.2 eV give rise to direct sensitivity to chemical bonding of organic materials. For example, near-edge X-ray absorption fine structure (NEXAFS) studies of neat P3HT and PCBM films have shown that the absorption is sensitive to small changes of the X-ray energy near the carbon absorption edge (280−320 eV).[14] The C 1s to π^* transition differs by 0.6 eV (285.1 eV for P3HT whereas two resonances at 284.5 and 285.8 eV for PCBM), such that scattering is enhanced at these energies where the absorption differs significantly. In addition, the presence and absence of resonant scattering at the oxygen absorption edge (525 eV) can be another source of scattering contrast given that only PCBM contains oxygen atoms. Thus, the subtle differences in the absorption between P3HT and PCBM near the C edge and differences in elemental composition can be used to generate scattering contrast between domains which vary in P3HT/PCBM composition using RSOXS.

Figure 1 presents the RSOXS intensity as a function of the in-plane scattering vector, q, performed at the carbon

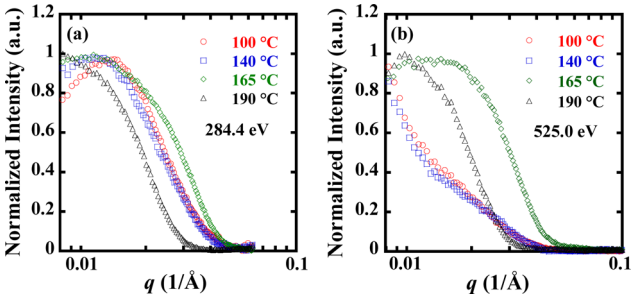

Figure 1. RSOXS intensity vs scattering vector, q, for 1:1 by mass P3HT/PCBM mixtures annealed at various temperatures for 30 min at (a) the carbon absorption edge (284.4 eV) and (b) the oxygen absorption edge (525 eV).

absorption (284.4 eV) and oxygen absorption (525 eV) edges for P3HT/PCBM mixtures annealed at variable temperatures. The intensities were normalized to compare the scattering profiles qualitatively. The broad peak or shoulder near 0.01−0.02 1/Å indicates the presence of a structure within the film. We note that the shape of scattering intensities at 284.4 eV shown in Figure 1a is analogous to that observed in previously reported GISAXS results for P3HT/PCBM mixtures in the hard X-ray regime (10 keV), suggesting that scattering is dominated by the structure factor of the morphology.[8e,15] Unfortunately, the use of a central stop for the CCD detector prevented the acquisition of accurate information at low scattering vectors (below 0.008 Å^{-1}), which is required to develop a reliable quantitative understanding of RSOXS data and to compare with GISAXS. Nevertheless, the RSOXS profiles at the carbon absorption energy (284.4 eV) display a gradual shift of peak positions toward the low q range with increasing annealing temperatures, suggesting that the structure of P3HT-rich domains coarsens upon annealing and the domain spacing grows. At the oxygen absorption edge (525 eV), however, the RSOXS profiles differ significantly with annealing temperature, indicating an energy dependence of the shape of the scattering profiles.

The comparisons of RSOXS profiles at 284.4 and 525 eV for films annealed at 190, 165, 140, and 100 °C are displayed in Figure 2. After annealing at 190 or 165 °C, we find that the

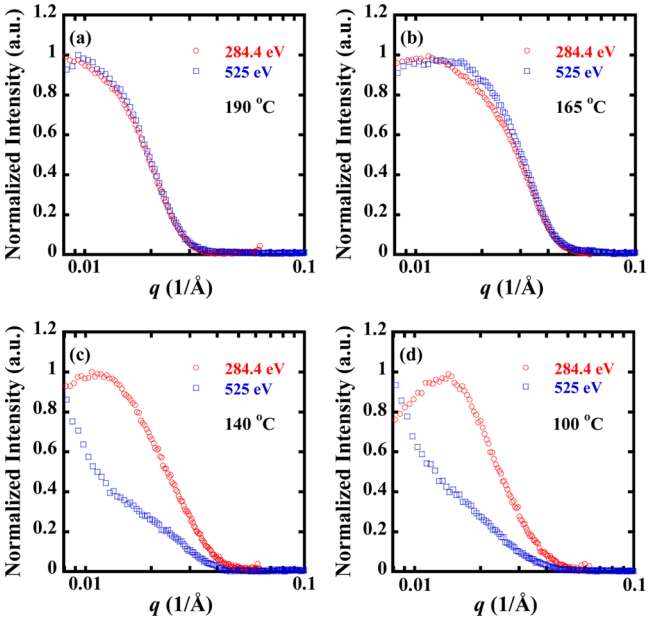

Figure 2. Comparison of RSOXS intensities vs scattering vector, q, at 284.4 and 525 eV for 1:1 by mass P3HT/PCBM mixtures annealed at (a) 190 °C, (b) 165 °C, (c) 140 °C, and (d) 100 °C for 30 min.

scattering profiles at the carbon (284.4 eV) and oxygen (525 eV) edges match, but after annealing at 140 or 100 °C the scattering profiles differ. The dependence of RSOXS data on the absorption edges at different X-ray energies results from the change in scattering contrast between domains. Thus, the scattering profiles at carbon and oxygen absorption energies are constant for P3HT/PCBM mixtures annealed at high temperatures regardless of the scattering contrast between domains, but the profiles are distinct for samples annealed at low temperatures.

The contrast variations observed in RSOXS studies must be related to differences in phase separation of P3HT/PCBM films under different processing conditions. That is, when two distinct domains are present modulating the scattering contrast does not change the shape of the scattering profiles (although the scattering intensities vary significantly). In contrast, when three or more distinct domains are present and the scattering contrast varies with the X-ray energy, then the scattering profiles can vary to reflect different periodicities associated with the different phases or domains. For example, RSOXS data at different X-ray energies reflect multiple periodicities when three distinct domains are present in triblock copolymers.[16] We will

dx.doi.org/10.1021/mz300547x | ACS Macro Lett. 2013, 2, 185−189

return to the origins of the variation in scattering contrast with X-ray energy below, after discussion of morphological characterization using energy-filtered TEM experiments.

Images of the active layer morphology of P3HT/PCBM mixtures annealed at 190 and 100 °C obtained from EFTEM are shown in Figure 3 as sulfur elemental maps. The difference

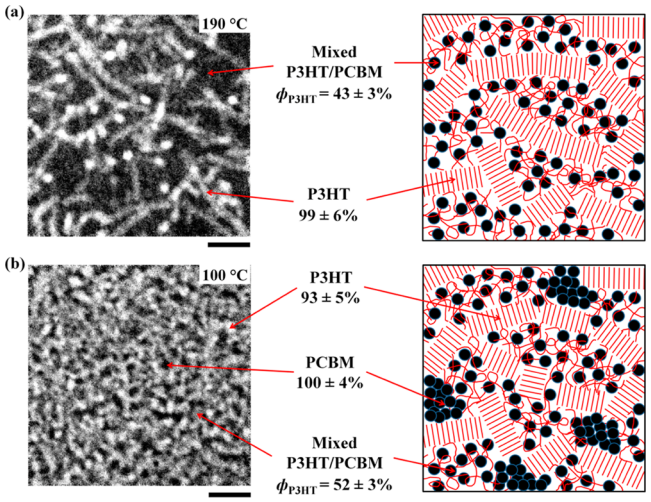

Figure 3. Sulfur elemental maps generated through EFTEM with schematic illustrations for 1:1 by mass P3HT/PCBM mixtures annealed at (a) 190 °C and (b) 100 °C for 30 min. The image intensity is proportional to the sulfur concentration. Therefore, the light regions correspond to P3HT-rich regions. The domain purity can be computed from the image intensities. The scale bar is 100 nm.

in sulfur composition of P3HT and PCBM generates high-contrast micrographs through inelastic scattering events. Because none of the major edges of the constituent elements (C, S, O, H) overlap, the intensity of the image is directly proportional to the total amount of sulfur[17] and can be translated to the concentration of P3HT within domains if the thickness of the film is known. Thus, the light regions in the image correspond to P3HT-rich domains, while the dark regions correspond to PCBM-rich domains. Figures 3a and 3b show the presence of P3HT fibers in a PCBM-rich matrix, although the structure of the film after annealing at 100 °C is significantly less defined than the structure after annealing at 190 °C.

For a two-component system A and B, the local domain purity in an elemental map can be computed from eq 2 based on the elemental density of the two components, $\rho_{i,A}$ and $\rho_{i,B}$ for element i

$$\phi_A(x, y) = \frac{(\bar{\phi}_A - k)}{\bar{I}_i} \frac{\bar{t}}{t(x, y)} I_i(x, y) + k \quad (2)$$

where $\phi_A(x, y)$ is the local volume fraction of component A integrated over the sample thickness; $\bar{\phi}_A$ is the average concentration of A in the sample; $k = \rho_{i,B}/(\rho_{i,B} - \rho_{i,A})$; $\bar{I}_i$ is the intensity averaged over the entire elemental map; $t(x, y)$ is the local relative thickness probed directly from the thickness map (assuming the mean free path is invariant for all components); $\bar{t}$ is the relative thickness averaged over the entire thickness map; and $I_i(x, y)$ is the local intensity of the elemental map. The thickness maps must be obtained from the same sample areas as the elemental maps. Equation 2 is only valid when the absorption edges do not overlap and, as such, is most useful for elemental maps generated from energy-filtered TEM images taken at core-loss energies. Given that sulfur is only present in P3HT ($k = 0$), a reduced equation can be used to map the local P3HT composition, $\phi_{P3HT}(x,y)$, from sulfur maps

$$\phi_{P3HT}(x, y) = \frac{\bar{\phi}_{P3HT}}{\bar{I}_S} \frac{\bar{t}}{t(x, y)} I_S(x, y) \quad (3)$$

$\bar{\phi}_{P3HT}$ is the average P3HT volume fraction in the film. Measurements of the fluorescence yield in NEXAFS experiments have demonstrated that the compositions of P3HT/PCBM films are equal to the compositions in solutions.[14] We assume that the composition of the imaged area is equal to the composition of the entire film; thus, $\bar{\phi}_{P3HT}$ is given by the P3HT/PCBM ratio in solution (0.58 volume fraction) prior to spin-coating. We note that this assumption is supported by the consistency of results obtained over many different images.[8e,18] After averaging results over 10 regions in the sulfur map of films annealed at 190 °C, we find that the volume fraction of P3HT is 0.43 ± 0.03 for PCBM-rich domains and 0.98 ± 0.05 for P3HT fibers perpendicular to the film surface (brightest circular regions in Figure 3a). A domain composition of 0.99 ± 0.06 P3HT by volume is obtained for the center of horizontal fibers by assuming one cylindrical fiber with diameter of around 20 nm in a PCBM-rich matrix. The domain concentrations were estimated in a similar way for films annealed at 100 °C as illustrated in Figure 3b. In this case, the images suggest that pure PCBM domains (1 ± 0.04) exist if we assume spherical PCBM aggregates in a P3HT/PCBM mixed matrix. Table S1 in the Supporting Information shows that similar results are obtained through analysis of the contrast using eq 2 in carbon maps (images not shown) instead of sulfur maps.

Our previous work demonstrates that three distinct phases are possible in P3HT/PCBM mixtures.[8e,18] P3HT will never fully crystallize, leaving an amorphous mixture of P3HT and PCBM as long as PCBM itself does not crystallize as a result of thermodynamic effects or processing. Nevertheless, amorphous P3HT and PCBM can phase separate if the interaction energy is high enough, leading to the formation of a nearly pure PCBM phase and a mixed P3HT/PCBM phase due to the asymmetric Flory–Huggins phase diagram.[8e] Hence, we conclude that at lower annealing temperatures (i.e., 100 °C) the sulfur map displays three phases including essentially pure P3HT (0.93 ± 0.05), pure PCBM (1 ± 0.04), and a mixture of amorphous P3HT and PCBM (ϕ_{P3HT} = 0.52 ± 0.03), obtained from the light, dark, and gray regions, respectively. We assume that the mixed phases are amorphous because no crystallization of PCBM or cocrystallization of P3HT and PCBM has been observed in our samples or in X-ray diffraction experiments for the processing conditions studied here.[11b,19] In particular, the bottom substrate can have a strong effect on the crystallization of PCBM,[20] and our samples are annealed as free-standing films (TEM) or on Si_3N_4 (RSOXS). As the annealing temperature increases to 190 °C, the increased miscibility of PCBM in P3HT[19b,21] could drive the mixture to form a two-phase system composed of essentially pure P3HT fibers (0.99 ± 0.06) and a PCBM-rich matrix phase (ϕ_{P3HT} = 0.43 ± 0.03).

The combination of the energy dependence of the RSOXS profiles (Figure 2) and the elemental maps from EFTEM (Figure 3) suggests that more than two phases exist at 100 and 140 °C, and only two phases exist at 165 and 190 °C. Length scales extracted from Fourier transforms of micrographs

dx.doi.org/10.1021/mz300547x | ACS Macro Lett. 2013, 2, 185–189

(Figure S1 of the Supporting Information) are in reasonable quantitative agreement with scattering results, although a full quantitative comparison which includes domain compositions requires further analysis and absolute scattering intensities. Furthermore, because 2D images are projections of 3D structures, interpretation of TEM micrographs can be convoluted when the density of features is high.[22] As a consequence, our analysis of domain compositions for images obtained after annealing at 100 °C, such as in Figure 3b, is speculative because we cannot rule out overlapping domains. RSOXS remains the most reliable method to characterize multiphase formation in thin-film mixtures of organic materials, and we note that our elemental maps are consistent with the RSOXS results.

We propose a hypothesis to explain how the scattering contrast is altered by the energy change based on the discovery of multiphase formation in P3HT/PCBM mixtures. Given the composition dependence of optical constants at soft X-ray energies, the mixed phase can be characterized with an average index of refraction weighted by its volume fraction. Thus, RSOXS can exploit differences in absorption between phases of distinct domain purities. For the two-phase system (190 °C) in Figure 3a, contrast is between pure P3HT and mixtures of amorphous P3HT and PCBM, which is independent of the absorption energy as evident in Figure 2a. Thus, the primary scattering peaks of RSOXS profiles probe information about the average domain spacing of P3HT regions.[15] For the three-phase system (100 °C), scattering data are composed of a superposition of scattering originating from periodicities corresponding to P3HT and PCBM-rich domains that can correspond to different length scales. Because the mixed phase (ϕ_{P3HT} = 0.52 ± 0.03) has a volume-averaged refractive index of the two components, contrast with either of the pure phases is similar, making extracting information about each individual phase challenging. At the oxygen absorption energy (525 eV, Figure 2d), for example, a weak feature around q = 0.015 Å^{-1} (40 nm) is barely identifiable. This length scale could correspond to the average domain spacing of P3HT-rich phases, which would be consistent with the structures observed with EFTEM imaging (see FFT analysis of elemental maps in Figure S1, Supporting Information) and previously reported GISAXS characterization.[8e] The upturn in intensities at low-q of the scattering data can be attributed to larger-scale structures and potentially macrophase separation. At the carbon absorption edge (284.4 eV), scattering corresponding to the shorter length scale (~40 nm) dominates. Thus, we speculate that contrast at 284.4 eV is mainly between pure P3HT against the integration of the other two phases (pure PCBM and mixtures of amorphous P3HT and PCBM).

We postulate that the strong enhancement of scattering from P3HT domains is due to the contrast in molecular orientation of crystalline P3HT fibers and amorphous P3HT in mixed phases. Recent work by Collins et al. has demonstrated that the orientational dependence of the index of refraction at the C 1s to π^* transitions can lead to scattering profiles which are dominated by the difference in orientation between domains.[23] The X-ray absorption at the π^* transition when the π orbitals are aligned with the X-ray polarization is three times the absorption of isotropically oriented π orbitals. In P3HT/PCBM mixtures, scattering from the crystalline domains (pure P3HT phases) would be enhanced at energies corresponding to the π^* transitions. As a result, the scattering contrast would differ at 284.4 eV from 525 eV, since no orientational dependence is expected at the oxygen edge. Hence, tuning the X-ray energy can modulate the contrast and provide evidence for the formation of multiple phases. In addition, RSOXS experiments with polarized X-rays may also elucidate orientational correlations, although a detailed analysis of the scattering contrast is impeded by the lack of a quantitative model describing the relationship between X-ray energy, X-ray polarization, and scattering contrast.

In summary, we have demonstrated the ability of RSOXS to characterize the multiphase formation in the active layer of organic solar cells. The strong resonant absorption of organic materials in the soft X-ray regime enables RSOXS to obtain high scattering contrast with chemical sensitivity and elemental selectivity. The energy dependence of the scattering profiles measured from P3HT/PCBM mixtures as a model system is consistent with the sulfur maps obtained through EFTEM. That is, the energy tuning afforded by RSOXS is able to modulate the scattering contrast generated between multiple phases, thus accessing structure information about different domains in P3HT/PCBM mixtures. Further, RSOXS characterization of the morphology in organic photovoltaics is potentially extendable to other combinations of organic materials or even much more complicated multiphase (>2) systems. For instance, multicomponent mixtures are difficult to fully investigate using hard X-ray techniques alone, while RSOXS may be a powerful tool to exploit contrast between each of the multiple components by tuning the X-ray energy to one or more resonance peaks corresponding to the chemistry of constituent organic materials.

■ ASSOCIATED CONTENT

Supporting Information

Materials and methods, domain compositions from elemental maps, and quantitative comparison between RSOXS and EFTEM data. This material is available free of charge via the Internet at http://pubs.acs.org.

■ AUTHOR INFORMATION

Corresponding Author

*E-mail: edg12@psu.edu.

Notes

The authors declare no competing financial interest.

■ ACKNOWLEDGMENTS

Funding from NSF under Award DMR-1056199 is acknowledged for this work. The authors also acknowledge support of the National Center for Electron Microscopy, Lawrence Berkeley National Laboratory, which is supported by the U.S. Department of Energy under Contract No. DE-AC02-05CH11231 and the Penn Regional Nanotechnology Facility, University of Pennsylvania. The Advanced Light Source is supported by the Director, Office of Science, Office of Basic energy Sciences, of the U.S. Department of Energy under Contract No. DE-AC02-05CH11231.

■ REFERENCES

(1) (a) Brabec, C. J. *Sol. Energy Mater. Sol. Cells* **2004**, *83*, 273−292. (b) Forrest, S. R. *Nature* **2004**, *428*, 911−918. (c) Gaudiana, R.; Brabec, C. *Nat. Photonics* **2008**, *2*, 287−289. (d) Shaheen, S. E.; Ginley, D. S.; Jabbour, G. E. *MRS Bull.* **2005**, *30*, 10−19.

(2) (a) Halls, J. J. M.; Walsh, C. A.; Greenham, N. C.; Marseglia, E. A.; Friend, R. H.; Moratti, S. C.; Holmes, A. B. *Nature* **1995**, *376*,

498−500. (b) Yu, G.; Gao, J.; Hummelen, J. C.; Wudl, F.; Heeger, A. J. *Science* **1995**, *270*, 1789−1791.
(3) (a) Dennler, G.; Scharber, M. C.; Brabec, C. J. *Adv. Mater.* **2009**, *21*, 1323−1338. (b) Hoppe, H.; Sariciftci, N. S. Polymer Solar Cells. In *Photoresponsive Polymers II*; Marder, S. R., Lee, K. S., Eds.; Springer: New York, 2008; Vol. *214*, pp 1−86. (c) McNeill, C. R. *Energy Environ. Sci.* **2012**, *5*, 5653−5667.
(4) Hoppe, H.; Niggemann, M.; Winder, C.; Kraut, J.; Hiesgen, R.; Hinsch, A.; Meissner, D.; Sariciftci, N. S. *Adv. Funct. Mater.* **2004**, *14*, 1005−1011.
(5) Hoppe, H.; Glatzel, T.; Niggemann, M.; Schwinger, W.; Schaeffler, F.; Hinsch, A.; Lux-Steiner, M. C.; Sariciftci, N. S. *Thin Solid Films* **2006**, *511*, 587−592.
(6) Li, G.; Shrotriya, V.; Yao, Y.; Huang, J. S.; Yang, Y. *J. Mater. Chem.* **2007**, *17*, 3126−3140.
(7) Lee, J. K.; Ma, W. L.; Brabec, C. J.; Yuen, J.; Moon, J. S.; Kim, J. Y.; Lee, K.; Bazan, G. C.; Heeger, A. J. *J. Am. Chem. Soc.* **2008**, *130*, 3619−3623.
(8) (a) Chiu, M. Y.; Jeng, U. S.; Su, C. H.; Liang, K. S.; Wei, K. H. *Adv. Mater.* **2008**, *20*, 2573−2578. (b) Collins, B. A.; Tumbleston, J. R.; Ade, H. *J. Phys. Chem. Lett.* **2011**, *2*, 3135−3145. (c) Giridharagopal, R.; Ginger, D. S. *J. Phys. Chem. Lett.* **2010**, *1*, 1160−1169. (d) Hoppe, H.; Sariciftci, N. S. *J. Mater. Chem.* **2006**, *16*, 45−61. (e) Kozub, D. R.; Vakhshouri, K.; Orme, L. M.; Wang, C.; Hexemer, A.; Gomez, E. D. *Macromolecules* **2011**, *44*, 5722−5726. (f) van Bavel, S.; Sourty, E.; de With, G.; Frolic, K.; Loos, J. *Macromolecules* **2009**, *42*, 7396−7403.
(9) (a) Pingree, L. S. C.; Reid, O. G.; Ginger, D. S. *Nano Lett.* **2009**, *9*, 2946−2952. (b) Yao, Y.; Hou, J. H.; Xu, Z.; Li, G.; Yang, Y. *Adv. Funct. Mater.* **2008**, *18*, 1783−1789.
(10) Yang, X. N.; Loos, J.; Veenstra, S. C.; Verhees, W. J. H.; Wienk, M. M.; Kroon, J. M.; Michels, M. A. J.; Janssen, R. A. J. *Nano Lett.* **2005**, *5*, 579−583.
(11) (a) Chu, C. W.; Yang, H. C.; Hou, W. J.; Huang, J. S.; Li, G.; Yang, Y. *Appl. Phys. Lett.* **2008**, *92*, 103306. (b) Woo, C. H.; Thompson, B. C.; Kim, B. J.; Toney, M. F.; Frechet, J. M. J. *J. Am. Chem. Soc.* **2008**, *130*, 16324−16329. (c) Kiel, J. W.; Eberle, A. P. R.; Mackay, M. E. *Phys. Rev. Lett.* **2010**, *105*, 168701. (d) Yin, W.; Dadmun, M. *ACS Nano* **2011**, *5*, 4756−4768.
(12) (a) Swaraj, S.; Wang, C.; Yan, H. P.; Watts, B.; Jan, L. N.; McNeill, C. R.; Ade, H. *Nano Lett.* **2010**, *10*, 2863−2869. (b) Virgili, J. M.; Tao, Y. F.; Kortright, J. B.; Balsara, N. P.; Segalman, R. A. *Macromolecules* **2007**, *40*, 2092−2099. (c) Yan, H. P.; Collins, B. A.; Gann, E.; Wang, C.; Ade, H.; McNeill, C. R. *ACS Nano* **2012**, *6*, 677−688.
(13) Gann, E.; Young, A. T.; Collins, B. A.; Yan, H.; Nasiatka, J.; Padmore, H. A.; Ade, H.; Hexemer, A.; Wang, C. *Rev. Sci. Instrum.* **2012**, *83*, 045110.
(14) Wang, H.; Gomez, E. D.; Kim, J.; Guan, Z. L.; Jaye, C.; Fischer, D. A.; Kahn, A.; Loo, Y. L. *Chem. Mater.* **2011**, *23*, 2020−2023.
(15) Vakhshouri, K.; Kesava, S. V.; Kozub, D. R.; Gomez, E. D. *Mater. Lett.* **2013**, *90*, 97−102.
(16) Wang, C.; Lee, D. H.; Hexemer, A.; Kim, M. I.; Zhao, W.; Hasegawa, H.; Ade, H.; Russell, T. P. *Nano Lett.* **2011**, *11*, 3906−3911.
(17) Egerton, R. F. *Electron Energy-Loss Spectroscopy in the Electron Microscope*, 2nd ed.; Plenum Press: New York, NY, 1996.
(18) Vakhshouri, K.; Kozub, D. R.; Wang, C. C.; Salleo, A.; Gomez, E. D. *Phys. Rev. Lett.* **2012**, *108*, 026601.
(19) (a) Gomez, E. D.; Barteau, K. P.; Wang, H.; Toney, M. F.; Loo, Y. L. *Chem. Commun.* **2011**, *47*, 436−438. (b) Treat, N. D.; Brady, M. A.; Smith, G.; Toney, M. F.; Kramer, E. J.; Hawker, C. J.; Chabinyc, M. L. *Adv. Energy Mater.* **2011**, *1*, 82−89.
(20) He, C.; Germack, D. S.; Kline, R. J.; Delongchamp, D. M.; Fischer, D. A.; Snyder, C. R.; Toney, M. F.; Kushmerick, J. G.; Richter, L. J. *Sol. Energy Mater. Sol. Cells* **2011**, *95*, 1375−1381.
(21) Collins, B. A.; Gann, E.; Guignard, L.; He, X.; McNeill, C. R.; Ade, H. *J. Phys. Chem. Lett.* **2010**, *1*, 3160−3166.
(22) Zhou, N. C.; Chan, C. D.; Winey, K. I. *Macromolecules* **2008**, *41*, 6134−6140.
(23) Collins, B. A.; Cochran, J. E.; Yan, H.; Gann, E.; Hub, C.; Fink, R.; Wang, C.; Schuettfort, T.; McNeill, C. R.; Chabinyc, M. L.; Ade, H. *Nat. Mater.* **2012**, *11*, 536−543.